Multi-Emissivity Setting in Thermal Imaging Based on Visible-Light Image Segmentation

Ding De-hong[1,a], Fang Kui*[1,b], Yu He-xiang[1], Qian Ke-jun[1] Chen Yi-neng[1], Cui Dai-jun[2]
[1]College of Resource & Environment, Hunan Agricultural University, Changsha, PR China
[2]Department of R & D, YADO Monitoring Technology Co. Ltd., Zhuhai, PR China
*Corresponding author, email: fk@hunau.net[b], dingdehong@qq.com[a]

Abstract

Emissivity is an accuracy influencing factor during infrared temperature measurement which focusing on regular geometry in laboratory under the condition of single emissivity. But in practical application, the target is often irregular with multi-emissivity,, and if following "idealized" method in laboratory, it will lead to inevitable error. This paper presents a method for a complex target object with the collection of multiple emissivities in infrared image after measurement. Both visible and infrared images were collected in the same field of view at the same time using binocular video to segment target regionally through visible image. The emission rate in corresponding region was set based on regional growing algorithm. Heat conduction equation was used as a reference to smooth the boundary area. After testing image evaluation parameters accordingly, results obtained via this infrared temperature measurement method are closer to the true value and precise compared with conventional ones judged from objective measurements.

Keywords: Multiple emissivity setting, edge extraction, region growing segmentation, boundary smooth transition base on equation of heat conduction

1. Introduction

There are mainly two blackbody radiation theories, Stefan - Boltzmann law and Planck radiation law which describes the relationship between the radiation rate and frequency of the electromagnetic radiation emitted from a blackbody, and the spectrum curves of blackbody radiation under different temperatures do not intersect. Stefan - Boltzmann law is as follows.

$$W = \varepsilon \sigma T^4 \tag{1}$$

All infrared temperature measuring devices are based on the principle that the surface temperature of objects can be accurately determined by measuring the infrared energy radiated by themselves. Blackbody is an idealized radiating body with a surface-emitting rate of 1. The radiation amount of actual objects existing in nature world depends on not only radiation wavelength and temperature of objects, but also type of material constituting object, surface roughness, physical and chemical structure, material thickness, preparation method, thermal process, surface state and environmental conditions etc [1]. For the application of blackbody radiation law to all actual objects, emissivity ε has been introduced as a coefficient related to material properties and surface state. This coefficient represents the approximation degree between heat radiation of actual objects and that of blackbody, and $\varepsilon \in (0,1)$. According to the law of radiation, the infrared radiation characteristics of any objects will be acquired as long as the emissivity of material is obtained.

The commonly used methods to determine the emission rate are Fourier transform infrared spectroscopy, double-reference method, dual-temperature method and dual background method, but they only target regular geometry and the results are single emissivity. Actually, the tested target is often of irregular geometry with the presence of multiple emissivities. If we follow the "ideal" laboratory method, a pre-set single emissivity will be necessary, which will lead to an inevitable error. Wang Pinqing [2] also pointed out that inaccurate emissivity has a significant impact on the tone display in geological infrared heat

map, but did not propose solutions. American scholars, Watson and Kahle [3-4], have recognized the influence of emissivity variation of ground objects and geological body on the calculation of surface temperature, considering that imaging using two thermal infrared bands (8-14 μm and 10.5-11.5 μm) can regulate the error of temperature calculation due to the changes of emissivity within the range 1%, the conclusion of which is in accordance with document [5]: for blackbody at 150 ℃, when measurement error of emissivity is 5%, the theoretical calculation error of measured temperature with thermal imager is up to about 1%.

It is also pointed out that [2] the actual surface temperature of different objects or geological bodies with the same tone (i.e. same radiation energy) in thermal infrared scanning image may vary considerably. For instance, water body at 27 ℃, quartz at 64 ℃ and marble at 32 ℃ may have the same radiation energy, i.e. same radiation temperature [6]. One of the methods infrared camouflage [7]—Making un-isothermal objects look isothermal, can be regarded as a example of reverse application involves emissivity. Generally, an emissivity difference of 0.01 among objects might result in an error of about 1 ℃ of radiation temperature. A method targeting complex object has been proposed in our study based on visible image segmentation technology, by setting multi-emissivity in infrared heat image afterwards, and can carry out infrared radiation thermometry more accurately.

2. Image Acquisition
2.1. Dual-channel Image Capture
Analysis and studies have shown that infrared thermal images (IR) and visible images (VI) are different in the following situations [8]: imaging of IR is based on the radiation caused by the temperature of object (passive imaging), while imaging of VI on the reflectivity of object (positive imaging); spatial resolution of IR is generally lower than that of VI. Grayscale of VI is more structured compared to IR's; texture details on the surface of scene can be reflected on VI but not IR. Edge characteristics in VI are evident with relatively steep edge while that of IR relatively smooth. Simultaneously, there is missing and offset phenomenon occurring at the edge of IR compared to VI for the same scene. Owing to the existence of more low-frequency components of IR, the correlation length of IR is larger than that of VI for the same scene.

2.2. Experimental Conditions
An online monitoring infrared camera (FLIR movement, DAHENG processor) purchased from Yado monitor company in Zhuhai City was used with a default emissivity of 0.95 and output mode of color selected as "Fusion". The indoor temperature of laboratory environment is 20 ℃, relative humidity 65%, and the room is without air convection with closed doors and windows. The size of aluminum block as research object is 20 * 10 * 5 mm with matte surface, and the intermediate was coated with paint into an irregular shape. After the block was placed in room for 2 hours for heat exchanging balance, shooting was conducted with respect to the same visual field. Figure 1 and 2 are VI and IR respectively under same visual field with a resolution of 320 * 240.

Figure 1. Visible-light image

Figure 2. Infrared thermograph

2.3. Issue Introduction
The aluminum block was maintained a consistent temperature as a whole by great thermal conductivity. It is obvious to be observed visually that, compared with temperatures

bands, the temperature of black paint amid the block is significantly higher than that of surrounding empty area by 4.4 measured with Yado's infrared camera, which means that the emissivity of these two regions is different. In other words, the emissivity of one object to be measured can not be simply fixed, getting rid of the method described in literature [5]. It is presented in this paper a method that multi-emissivity is set according to regions and how to shoot isosbestic infrared image for isothermal objects. Technology and methods involved are described as follows.

3. Edge Definition Based on Visible Light Image Segmentation

Partition the visible image because of the distinctive edge characteristics of VI. Image segmentation is separating image into different regions of specific meanings and disjoint, and each region is of the consistency of specific area. A image g (x, y) segmentation is dividing image into sub region g1, g1 and g3 meeting the following conditions:

$\mathbf{U}_{k=1}^{N} g_k(x,y) = g(x,y)$ I.e., all regions comprise the whole image.

g_k is a region in communication.

$g_k(x,y) \mathbf{I} \ g_j(x,y) = \varphi$ I.e., two arbitrary sub regions have nothing in common.

Region g_k is of uniformity to a certain extent, which refers to small difference or slow changes of grayscale value between the pixels within the same region.

There are many methods for image segmentation, and not an individual image segmentation algorithm but the combination of several methods are applied to achieve perfect image segmentation effect [11-12]. Classic methods include threshold segmentation [9-10], edge detection method [13], statistical segmentation method [14] and the method of combining region and boundary information. In addition, there are many other methods and literatures in the field of image segmentation, such as image segmentation based on partial differential equation [15], image segmentation based on genetic algorithm [16], image segmentation method based on wavelet analysis and transform [17-18], image segmentation method based on mathematical morphology [19], image segmentation method based on fuzzy theory [20-21], image segmentation method based on artificial neural network [22]. The black region in Figure 1 was segmented using Canny detector with the aid of MATLAB [23] in this paper. The procedures are:

Image is smoothed by a Gaussian filter with specified standard deviation σ to reduce the noise.

Local gradient $g(x,y) = [G_x^2 + G_y^2]^{1/2}$ and edge direction $\alpha(x,y) = \arctan(G_y / G_x)$ are calculated at each point; edge point is defined as the point of maximum local strength in gradient direction.

Edge points defined in item (b) will result in ridge in gradient magnitude image. Then, the algorithm tracks top of all the ridges and set all pixels not at the top of ridge to zero in order to create a thin line in the output, which is well-known as non-maximum resisting treatment. Pixels at the ridge are set using two threshold values $T1$ and $T2$ ($T1 < T2$): ridge pixel is called strong edge pixel when the value is greater than T2 while called weak edge pixel when between $T1$ and $T2$.

Finally, the algorithm integrates weak pixels connected by 8 pixels into strong pixels and performs edge linking.

Canny edge detector is performed using the following syntax:

$$[g, \ t] = \text{edge} (f, \text{'canny'}, T, \text{sigma}) \tag{2}$$

where T is a vector and $T = [T1, T2]$. Sigma is the standard deviation of smoothing filter with a default of 1.

Procedures of edge extraction from VI then superimposed with IR in Matlab are described as follows:

```
rgb=im2double(imread('IR_1.jpg'));
IR=imread('VI.jpg');
I=rgb2grayscale(IR);
```

```
K=imadjust(I,[20/255 1]);  % contrast enhancement
Ir_edge=edge(K, 'canny',[0.04 0.50],1);
r=rgb(:,:,1).*~Ir_edge;
g=rgb(:,:,2).*~Ir_edge;
b=rgb(:,:,3).*~Ir_edge;
r(Ir_edge)=1;  % edge set as white
g(Ir_edge)=1;
b(Ir_edge)=1;
result=cat(3,r,g,b);
```

Figure 3 is the extracted edge and Figure 4 the result of regional definition after superposition of Figure 2 and 3.
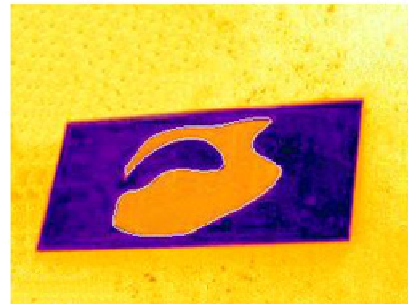

Figure 3. Extraded edge   Figure 4. Infrared thermograph after regional definition

4. Multi-Emissivity Setting According to Region

The following conclusions can be drawn from the comparison of Figure 2, for instance, and equation 1: under ideal condition, W is a constant and T is inversely proportional to ε. If actual emissivity is higher than the one set by instruments, the measured temperature will be excessively high, and lower actual emissivity will lead to lower measured temperature, on the other hand. High value turns higher and low value lower. A greater error of ε will cause more chromatic aberration. In other words, chromatic aberration of heat map is larger than the actual. After setting emissivity according to region chromatic aberration should be reduced, and the whole aluminum block in Figure 2 should be in the same uniform color under ideal circumstances.

a) Determination of emissivity

Paint of a known emissivity was evenly sprayed on the surface of tested object, and then adjusted the emissivity of infrared camera until the exposed and painted surface reached a same or close temperature. Emissivity at this time is the correct one of the target [24].

b) Multi emissivity setting on the basis of region growing algorithm

Emissivity (*Es*) of the paint is 0.99 by looking up relevant table and that of non-paint part Emissivity (*Er*) 0.3 determined by the above experimental methods. After the setting of painted part emissivity with *Es* and non-paint with Er respectively region growing algorithm was used with Matlab [23]:

Q= True; Absolute value of grayscale difference between pixels of seeds and a point $(x, y) \leq T$

Q= False; Other situations

The first step is to determine seed, which is conducted with mouse (command "getpts" in Matlab) manually. Then, all the pixels corresponding to the following conditions were attached to each seed to form growing area: (a) connected to seed in the form of 8, and (b) similar to the seed. T is a designated threshold value, although this feature is based on grayscale-scale difference and relatively unitary. A more complicated scheme is formulated in this research that the corrected grayscale heat map is derived via reverse derivation according to the two different emissivity (Es and Er) and original grayscale scale image, and then converted to pseudo-color

image. As a result, the paint part shifts to color blue and non-paint portion to color orange. Owing to the varied fitting equations correlating grayscale with temperature of various detectors, even the identical detector, parameters employed by fitting equation will change in different situations, so the expatiatory quantitative calculation process is ignored here, and the results are shown in Figure 5 and 6, both of which are superposed to form Figure 7. Chromatic aberration of both regions is significantly reduced visually and the pseudo-color image tends to consistency, but obvious boundary defects are observed, which is because pixels at the junction belong to neither Figure 5 nor Figure 6.

Figure 5. Non-pain region　　　Figure 6. Painted region　　　Figure 7. Superimposition of two regions

5. Smooth Transition of "Color Temperature" at Stitching Place using heat Conduction Equation

Joseph · Fourier describes a general heat conduction model in his published work "analytic thermology" in 1822:

$$u_t = ku_{xx}$$

The x is spatial variable $\in [0,1]$ indicating the normalized length, and t is time variable, where

k = .061644 subject to the boundary conditions:

$$u_x(0,t) = 0 = u_x(1,t)$$

and with the initial heat distribution given by:

$$u(x,0) = \cos(2x)$$

In this case, the left face (x=0) and the right face (x=1) are perfectly insulated. This image shows how the heat redistributes, flowing from the warmer left edge to the cooler right edge, then equalizing to a constant temperature throughout. This temperature happens to be the average value of cos(2x) over [0,1], as one might expect.

The solution [25]:

$$u(x,t) = \frac{\sin(2)}{2} + \sum_{n=1}^{\infty} A_n \cos(n\pi x) \exp(-kn^2\pi^2 t)$$

Where:

$$A^n = 2\int_0^1 \cos(2x)\cos(n\pi x)dx = (-1)^n \frac{-4\sin(2)}{n^2\pi^2 - 4}$$

A transient thermal conductivity curve is shown in Figure 8 at some time-point. The curve becomes flatter as evolution and horizontal when reaching thermal equilibrium.

It is hard to make the "colorful temperature"(which weighs the temperature by color)of painting area as the totally same as that of non-painting area, due to the error of the emissivity or effect of precision. If the two areas are the same completely, the result seems to be not reality. But they should be the same on the theory, which means finding a way to make the colorful temperature on the boundary transit smoothly. The figure 8 provides the reference to solve this question. The situation of figure 7 could imitate as the way of heat conduction: the heat conduction has already reach some balance that there is no change on transition band between high-temperature zone and the low-temperature zone. Specifying that T2 indicates the

high-temperature in painting area and T1 represents the low-temperature of non-painting area. As the result of that, temperature of transition area, from the intrinsic to extrinsic, should from T2 to T1 smoothly according to the heat conduction equation. Choosing when and which part of curve, it is not sure. On the sake of the difference between T1 and T2 is small, we can use direct- line instead of Cn-C1 in this paper.
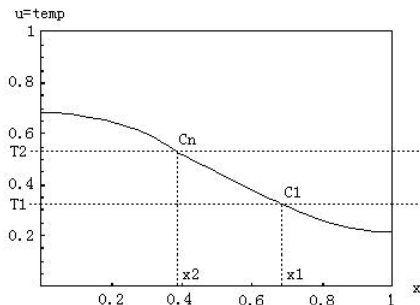

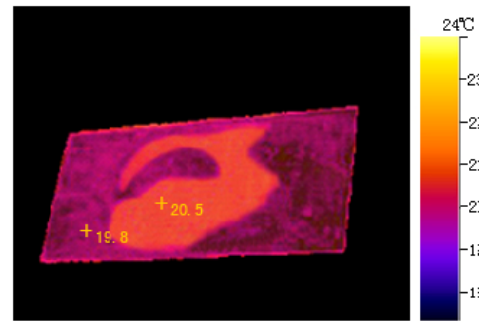Figure 8. Transient heat conduction curve

Figure 9. Heat map after smooth transition for boundary

The procedure using Matlab to implement this algorithm is: expand the contour line to a width of n pixels (the original is 1 pixel wide), and n is an odd number to exactly cover the vacant points at splicing. n = 5 in this paper actually. Loop point-by-point along the original contour and find line segments Li with a length of n at point i perpendicular to contour line (node coordinates of Li from outside to inside: Ci1 ... Cin; and contour line at the midpoint: Cin/2 + 1). It can be obtained from Figure 8 that TCi1 = T2 and TCin = T1. Then divide line segment Li into n-1 equal parts to deduce temperatures of other points. After processing, the result is shown in Figure 9 and the main pseudo-code is given by:

```
For  i = 1: M   // Loop point-by-point along the original contour
        Solve line segment Li
        TCi1 = T2, TCin = T1
         For  j = 2: n-1      // calculate color and temperature of n-2 points in the line Li
             TCij = TCi (j-1) + (T2-T1)/(n-1)
             Reversely calculate grayscale value Grayscale-i according to TCij
             Calculate color Color-i at the point according to Grayscale-i
             Set the color at Cij to Color-i
        End;
End;
```

6. Experimental Results and Parameters Test

Referring to characteristic properties of texture statistics [8], evaluate the grayscale components of Figure 2 and 8 by citing the following statistical characteristics:

Information entropy: Information entropy of image is an important indicator measuring the information richness in images and the size of which reflects the average amount of information contained in images, which is defined as

$$H = -\sum_{i=0}^{L-1} P_i \log_2 P_i$$

, where Pi is the distributional probability of grayscale i in the range of $[0,1,\mathrm{L}\ ,L-1]$. Greater entropy means richer information of an image.

Standard deviation: It represents the discretion extent between image grayscale and average grayscale, which is defined as

$$\sigma = \sqrt{\frac{\sum_{m=0}^{M-1}\sum_{n=0}^{N-1}[F(m,n)-\overline{F}]^2}{M*N}}$$

where $\overline{F}$ is the average grayscale of the whole image. A larger standard deviation will lead to more dispersed image grayscale distribution and greater image contrast, and more information will be extracted. On contrary, concentrated image grayscale distribution will result in smaller contrast and less information.

Contrast: Contrast refers to the grayscale ratio of bright and dark parts on screen, which is given by:

$$c = \sum r(i,j) \cdot r(i,j) \cdot p(i,j)$$

$r(i,j) = |i-j|$ grayscale difference between adjacent pixels; $p(i,j)$ the pixel distributional probability of gray-scale difference of r between adjacent pixels.

Smoothness: Smoothness characteristics [26] is based on grayscale histogram h (n):

$$S(h) = \sum_{i=0}^{254} |h(i) - \frac{h(i-1)+h(i+1)}{2}| + |h(0)-h(1)| + |h(255)-h(254)|$$

This parameter can illustrate, to a certain extent, the distributional smoothness of grayscale histogram. If the histogram distribution is uniform, the calculated characteristic value will be small.

Third moment: The skewness of histogram can be measured by this parameter. If the histogram is symmetrical, the value is 0. If it is positive, histogram skews right, and if negative, skews left.

$$\mu_3 = \sum_{i=0}^{L-1}(z_i - m)^3 p(z_i)$$

Consistency: When all grayscale values are equal, this parameter reaches acme and decreases in other situations.

Tested by "Crop Image Analysis System Program"[27], it can be concluded from Table 1 that entropy, standard deviation, contrast and third moment are all smaller in Figure 9 than those in Figure 2 except for consistency and smoothness, meaning that heat map demonstrates greater uniformity, smoothness and consistency, namely heat map of aluminum block with the emissivity set according to regions, almost a whole, and objective evaluation is consistent with subjective evaluation.

Table 1. Comparison of parameters for evaluation

Parameters	Figure 2	Figure 9	Variance
Temperature difference(℃)	4.4	0.7	↓
Entropy (e)	6.28666	5.09708	↓
Standard deviation(σ)	0.33481	0.25940	↓
Contrast (c)	0.15223	0.11496	↓
Smoothness S(h)	0.00831	0.04782	↑
Third moment($\cup 3$)	2.55723	0.18665	↓
Consistency U	0.01669	0.04644	↑

7. Conclusion

This paper presents a method using improved region growing algorithm with setting distinct emissivity at different locations through edge extraction based on visual image and then superimposing the edge on infrared heat map. With the aid of heat conduction equation, smooth transition zone to make the heat hologram indicate real temperature more precisely.

Comparison Figure 9 with Figure 2, painted and non-paint regions tend to be more consistent after processing, confirmed with experimental measured parameters. This method is extremely appropriate for the heat monitoring of combination and mixture, such as monitoring respiration and heat release of different seeds under the same ambience for nurturing, and camouflage/anti-camouflage. Further engineering conversion will be required for applying this research results to engineering practice under complex geological circumstances.

References
[1]   Ye yutang. Infrared and Low Light Level Technology. Beijing:National Defense Industrial Press. 2010: 22-25.
[2]   Wang pinqing. The Effect of Emissivity on Thermal's image and It's Interpretation. *Remote sensing of environment*. 1988; 15: 207-212.
[3]   Alan R, Gillespie, Anne B, Kahle. Construction and Interpretation of a Digital Thermal Inertia Image. *Photogrammetric Engineering and Remote Sensing*. 1977; XL111(8): 938-999.
[4]   SH Miller, Kennech Watson. *Evaluation Algorithms for Geological Thermal-Inertia-Mapping*. Proceedings of the 11th International symposium on Remote Sensing of Environment. 1977; 11: 1147-1160
[5]   Lu zifeng. Calibration and the measurement error analysis of infrared imaging system for temperature measurement. Dissertation. Beijing: Chinese Academy of Sciences; 2009.
[6]   Konrad JK, Buettner Clifford D Kern. The determination of infrared emissivities of terrestrial surfaces. *Journal of Geophysical Research*. 1965; 70: 1329-1337.
[7]   YU Da-bin. Effect of infrared emissivity of coatings on the camouflage effectiveness of targets. *Infrared and Laser Engineering*. 2007; 36: 194-197.
[8]   Li junshan. Infrared Image Processing, Analysis and Fusion. Beijing: Science Press. 2009: 11-13.
[9]   Cheng HD, Li JG, Chen JR. Threshold selection based on fuzzy c-partition entropy approach. *Pattern Recognition*. 1998; 31: 857-870.
[10] Jui-Cheng Yen, Fu-Juay Chang. A New Criterion for Automatic Multilevel Thresholding. *IEEE Transaction Image Processing*.1995; 4: 370-378.
[11] Hanshan Li,Zhiyong Lei.Research on Infrared Special Facula View Measurement Method Based on Image Processing Technology. *TELKOMNIKA Indonesian Journal of Electrical Engineering*. 2012; 10(6): 1422-1429.
[12] Li Zhengzhou etc.Gray-scale Edge Detection and Image Segmentation Algorithm Based on Mean Shift. *TELKOMNIKA Indonesian Journal of Electrical Engineering*. 2013; 11(3): 1414-1421.
[13] Legault R, Suen CY. Optimal local weighted averaging methods in contour smoothing. *IEEE Transactions on Pattern Analysis and Machine Intelligence*. 1997; 19: 801-817.
[14] Giordana N, Pieczynski W. Estimation of generalized multisensory hidden Markov chains and unsupervised image segmentation. *IEEE Transactions on Pattern Analysis and Machine Intelligence*. 1997; 19: 465-475.
[15] Zhang tan, Chen gang. Image processing based on partial differential equation. Beijing: Higher education press. 2004.
[16] Tian Ying, Yuan Wei-qi. Application of the Genetic algorithm in image Processing. *Journal of Image and Graphics*. 2007; 12: 389-396.
[17] Yansun Xu, Weave JB. Wavelet transform domain filters: a spatially selective noise filtration technique. *IEEE Transactions on Image Processing*. 1994; 3: 747-758.
[18] Mallat S, Hwang WL. Singularity detection and processing with wavelets. *IEEE Transactions on Information Theory*. 1992; 38: 617-643.
[19] Deng Shiwei, Yuan Baozong. Range Image Segmentation Based on Mathematical Morphology. *Acta Electronica Sinica*. 1995; 23: 6-9.
[20] LUO Shu-qian, TANG Yu. A Bias Based Adaptive Fuzzy Segmentation Algorithm. *Journal of Image and Graphics*. 1999; 7A: 111-114.
[21] XUE Jinghao, ZHANG Yujin, LIN Xinggang. *New thresholding algorithm based on fuzzy divergence for image segmentation*. Beijing: Tsinghua Univ (Sci&Tech). 1999; 39: 47-50.
[22] Kuntimad G, Ranganath HS. Perfect image segmentation using pulse coupled neural networks. *IEEE Transactions on Neural Networks*. 1999; 10: 591-598.

[23] Gonzalez HC. Digital Image Processing Using MATLAB. 3rd ed. Beijing: Publishing House of electronics industry. 2005: 289-293.

[24] Qi wenjuan. Effect of emissivity on accuracy of infrared temperature measurement. Thesis. Changchun university of science and technology. 2006.

[25] Electronic   Publication: Wikipedia. http://commons.wikimedia.org/wiki/File:Heatequation_exampleB.gif?uselang=zh.

[26] WANG Ran, PING Xi-jian. Steganalysis of LSB Matching Based on Local Smoothness of Histogram. *Journal of Applied Sciences in Shanghai*. 2012; 30: 96-103.

[27] Jinwei Li, Guiping Liao. Crop Image Analysis System Program Ver2.0